http://dx.doi.org/10.5012/bkcs.2013.34.1.167

Highly Efficient Red Emissive Heteroleptic Cyclometalated Iridium(III) Complexes Bearing Two Substituted 2-Phenylquinoxaline and One 2-Pyrazinecarboxylic Acid

Nallathambi Sengottuvelan,[a] Seong-Jae Yun, Dae-Young Kim, In-Hye Hwang, Sung Kwon Kang,[†] and Young-Inn Kim[*]

Department of Chemistry Education and Interdisciplinary Program of Advanced Information and Display Materials, Pusan National University, Pusan 609-735, Korea. [*]E-mail: yikim@pusan.ac.kr
[†]Department of Chemistry, Chungnam National University, Daejeon 305-764, Korea
Received September 20, 2012, Accepted October 25, 2012

A series of highly efficient red phosphorescent heteroleptic iridium(III) complexes **1-6** containing two cyclometalating 2-(2,4-substitued phenyl)quinoxaline ligands and one chromophoric ancillary ligand were synthesized: $(pqx)_2Ir(mprz)$ (**1**), $(dmpqx)_2Ir(mprz)$ (**2**), $(dfpqx)_2Ir(mprz)$ (**3**), $(pqx)_2Ir(prz)$ (**4**), $(dmpqx)_2Ir(prz)$ (**5**), $(dfpqx)_2Ir(prz)$ (**6**), where pqx = 2-phenylquinoxaline, dfpqx = 2-(2,4-diflourophenyl)quinoxaline, dmpqx = 2-(2,4-dimethoxyphenyl)quinoxaline, prz = 2-pyrazinecarboxylate and mprz = 5-methyl-2-pyrazinecarboxylate. The absorption, emission, electrochemical and thermal properties of the complexes were evaluated for potential applications to organic light-emitting diodes (OLEDs). The structure of complex **2** was also determined by single-crystal X-ray diffraction analysis. Complex **2** exhibited distorted octahedral geometry around the iridium metal ion, for which 2-(2,4-dimethoxyphenyl)quinoxaline N atoms and C atoms of orthometalated phenyl groups are located at the mutual trans and *cis*-positions, respectively. The emission spectra of the complexes are governed largely by the nature of the cyclometalating ligand, and the phosphorescent peak wavelengths can be tuned from 588 to 630 nm with high quantum efficiencies of 0.64 to 0.86. Cyclic voltammetry revealed irreversible metal-centered oxidation with potentials in the range of 1.16 to 1.89 V as well as two quasi-reversible reduction waves with potentials ranging from −0.94 to −1.54 V due to the sequential addition of two electrons to the more electron-accepting heterocyclic portion of two distinctive cyclometalated C^N ligands.

Key Words : Iridium(III) complexes, Photoluminescence, Highly efficient red phosphorescence, Color tuning

Introduction

Phosphorescent heavy-metal complexes as emitters in organic light-emitting diodes (OLEDs) have attracted increasing attention because they can fully utilize both singlet and triplet excitons through the strong spin-orbital coupling of heavy-metal ions.[1] Most recently, considerable effort has been focused on the design of OLEDs based on phosphorescent cyclometalated iridium complexes owing to their relatively short excited-state life time, high photoluminescence efficiency and excellent wavelength tunability over the entire visible spectrum, and an internal phosphorescence quantum efficiency (η_{int}) as high as ~100% can theoretically be achieved.[2] On the other hand, there are a few red-emitting iridium complexes, which are important for the realization of RGB full-color displays and the creation of white organic light-emitting devices (WOLEDs).[3] Compared to green and blue phosphorescent iridium complexes, red emitting iridium complexes tend to have limited quantum yields[4] due to the energy gap law. Increasing the vibrational overlap between the excited and ground states causes an increase in non-radiative rates (k_{nr}) and a decrease in the radiative rates (k_r) for longer wavelength emission, resulting in lower quantum efficiency in red emitters. Therefore, the synthesis of new highly efficient red emitting materials is generally based on the design of rigid cyclometalated ligands with a low degree of freedom for vibrational loss. Recently, the highly efficient heteroleptic cyclometalated iridium(III) complexes bearing nitrogen containing 2-phenylquinoxaline-based ligands with a low degree of freedom were reported.[5] The reported complexes emitted from red-orange to deep red phosphorescence with high emission quantum yields (Φ = 0.58-0.78) were found to be dependent on the substituent of cyclometalated ligands, and were suggested to be good triplet phosphors for OLEDs applications.

As part of an ongoing study of highly efficient red-emitting materials, this paper reports synthesis and characterization of a series of six red-emitting iridium(III) complexes containing two substituted 2-phenylquinoxaline ligands and one 2-pyrazinecarboxylic acid. The energy gap between the ground and lowest excited states can be reduced effectively by either an extension of p electron delocalization of the aromatic ligand chromophore or by emission from a nitrogen containing 2-pyrazinecarboxylate ancillary ligand, giving emitters with highly efficient red color due to an intra-ligand energy transfer (ILET) process.

[a]Current address: Department of Chemistry, Alagappa University, Karaikudi, 630003, India

Experimental

Materials. All reagents and solvents were obtained commercially from Sigma-Aldrich Chemicals or Acros Organics, and used as received with the exception of tetrahydrofuran (THF), which was distilled from sodium/benzophenone under nitrogen.

Synthesis of Ligands: 2-Phenylquinoxaline (pqx). 2-Phenylquinoxaline (pqx) was prepared from a reaction of 2-chloroquinoxaline and phenylboronic acid. 2-Chloroquinoxaline (3.00 g, 18.2 mmol), phenylboronic acid (2.44 g, 20.0 mmol) and tetrakis(triphenylphosphine)palladium(0) (0.98 g, 0.85 mmol) were added to 50 mL of THF. After adding 5 mL of aqueous 4 M K_2CO_3, the reaction mixture was heated to 80 °C for 24 h. The cooled crude mixture was poured into water, extracted with CH_2Cl_2 (50 mL × 3 times) and dried over anhydrous magnesium sulfate. Finally, silica column purification (*n*-hexane:EtOAc = 5:1) gave 3.15 g of a white solid in quantitative yield (84%). mp 77 °C. ^{1}H NMR δ 7.55 (m, 3H), 7.73 (m, 2H), 8.09 (m, 4H), 9.34 (s, 1H).

2-(2,4-Dimethoxyphenyl)quinoxaline (dmpqx). 2-(2,4-Dimethoxyphenyl)quinoxaline (dmpqx) was prepared in a similar manner as 2-phenylquinoxaline (pqx) except that 2,4-dimethoxyphenylboronic acid was used instead of phenylboronic acid. Yellow crystals were obtained. Yield: 3.75 g (77%). mp 75 °C. ^{1}H NMR δ 3.90 (s, 6H), 6.61 (s, 1H), 6.69 (d, 1H), 7.71 (m, 1H), 7.91 (d, 2H), 8.08 (m, 2H), 9.35 (s, 1H).

2-(2,4-Difluorophenyl)quinoxaline (dfpqx). 2-(2,4-Difluorophenyl)quinoxaline (dfpqx) was prepared using 2,4-difluorophenylboronic acid instead of phenylboronic acid. A white solid was obtained. Yield: 3.80 g (87%). mp 90 °C. ^{1}H NMR δ 7.13 (m, 1H), 7.17 (m, 2H), 7.91 (m, 2H), 8.27 (m, 2H), 9.45 (s, 1H).

Synthesis of Iridium Complexes: General Procedure. Cyclometalated iridium(III) μ-chloro-bridged dimer, $[(C\hat{}N)_2Ir(\mu\text{-}Cl)]_2$, where C^N = pqx, dmpqx and dfpqx, were prepared from a reaction of iridium chloride trihydrate (2.00 g, 5.67 mmol) and the C^N ligand (17.01 mmol) in a mixture of water (10 mL) and 2-ethoxyethanol (30 mL) at 135 °C under a nitrogen atmosphere for 30 h. The reaction mixture was allowed to cool to room temperature and treated with water (30 mL) to induce the precipitation of a brown solid. The solid was filtered and washed with water, hexane and diethyl ether. The product portion was collected and dried under vacuum. The μ-chloro-bridged dimer $[(C\hat{}N)_2Ir(\mu\text{-}Cl)]_2$ (0.39 mmol), sodium carbonate (0.414 g, 3.90 mmol) and 3 equivalent ancillary N^O ligand, where N^O = 5-methyl-2-pyrazinecarboxylic acid (mprz) and 2-pyrazinecarboxylic acid (prz) were dissolved in 30 mL of 2-ethoxyethanol. After degassing, the reaction vessel was maintained under nitrogen. The temperature was increased to 130 °C and the reaction mixture was stirred for 20 h. The resulting dark solution was concentrated under vacuum at 60 °C, and the residues were eluted through a silica column.

$[(pqx)_2Ir(mprz)]$ (1). Red solid. Yield: 0.18 g (62%). ^{1}H NMR ($CDCl_3$, 400 MHz) δ 2.52 (s, 3H), 6.12 (d, 2H), 6.7 (t, 2H), 6.83 (dd, 2H), 7.01 (m, 2H), 7.53 (m, 2H), 7.65 (m, 2H), 7.98 (d, 2H), 8.07 (m, 2H), 8.64 (d, 2H), 8.90 (s, 1H), 9.49 (d, 1H).

$[(dmpqx)_2Ir(mprz)]$ (2). Dark red solid. Yield: 0.16 g (56%). ^{1}H NMR ($CDCl_3$, 400 MHz) δ 2.54 (s, 3H), 3.23 (d, 6H), 3.93 (d, 6H), 5.30 (s, 1H), 5.98 (ddd, 2H), 6.93 (m, 2H), 7.06 (d, 1H), 7.42 (ddd, 1H), 7.53 (m, 1H), 7.76 (s, 1H), 7.95 (m, 2H), 8.54 (m, 1H), 8.89 (s, 1H), 10.14 (d, 2H).

$[(dfpqx)_2Ir(mprz)]$ (3). Orange solid. Yield: 0.12 g (42%). ^{1}H NMR ($CDCl_3$, 400 MHz) δ 2.49 (s, 3H), δ 5.63 (dd, 2H), 6.32 (dd, 2H), 6.61 (m, 2H), 6.69 (m, 1H), 7.02 (dd, 1H), 7.49 (s, 1H), 7.89 (d, 1H), 8.21 (q, 2H), 8.79 (s, 1H), 9.15 (s, 1H), 9.79 (dd, 2H).

$[(pqx)_2Ir(prz)]$ (4). Red solid. Yield: 0.14 g (49%). ^{1}H NMR ($CDCl_3$, 400 MHz) δ 6.19 (d, 2H), 6.70 (t, 2H), 6.82 (m, 2H), 7.01 (m, 2H), 7.15 (ddd, 2H), 7.55 (m, 2H), 7.85 (m, 2H), 8.01 (d, 2H), 8.10 (m, 1H), 8.64 (m, 1H), 9.08 (s, 1H), 9.50 (d, 2H).

$[(dmpqx)_2Ir(prz)]$ (5). Dark red solid. Yield: 0.16 g (57%). ^{1}H NMR ($CDCl_3$, 400 MHz) δ 3.23 (d, 6H), 3.99 (d, 6H), 5.30 (s, 1H), 5.99 (ddd, 2H), 6.93 (t, 2H), 7.04 (d, 2H), 7.39 (t, 1H), 7.52 (m, 1H), 7.95 (m, 2H), 8.51 (m, 1H), 8.65 (d, 1H), 9.01(s, 1H), 10.14 (d, 2H).

$[(dfpqx)_2Ir(prz)]$ (6). Orange solid. Yield: 0.19 g (67%). ^{1}H NMR ($CDCl_3$, 400 MHz) δ 5.61 (dd, 2H), 6.29 (dd, 2H), 6.55 (m, 2H), 6.71 (m, 1H), 6.98 (dd, 1H), 7.52 (s, 1H), 7.96 (d, 1H), 8.11 (q, 2H), 8.56 (d, 1H), 8.75 (s, 1H), 9.05 (s, 1H), 9.83 (dd ,2H).

Instruments. The ^{1}H nuclear magnetic resonance (NMR, Varian Mercury 300 MHz instrument) spectra were recorded and the chemical shifts were referenced to $CDCl_3$ as an internal standard. The UV-visible spectra were recorded on a Jasco V-570 UV-vis. spectrophotometer and the photoluminescence (PL) spectra were recorded at room temperature using a Hitachi F-4500 fluorescence spectrophotometer in the range of 400-800 nm. $Ir(ppy)_3$, where ppy is 2-phenylpyridine, was used as the reference, assuming a quantum yield of 0.40 with 360 nm excitation, to determine the luminescence quantum yield of the studied compounds in a CH_2Cl_2 solution. The solution samples were degassed by three freeze pump-thaw cycles. The resulting luminescence was measured using an intensified charge-coupled detector. Electrochemical measurements were performed using a Bioanalytical Systems CV-50 W electrochemical analyzer with a three electrode cell assembly. The electrochemical cell consisted of a glassy carbon working electrode, platinum wire counter electrode and Ag/AgCl reference electrode. The oxidation and reduction measurements were recorded in a CH_2Cl_2 solution containing tetra(*n*-butyl)ammonium hexafluorophosphate as the supporting electrolyte at a scan rate of 50 mV s^{-1} under nitrogen conditions. Each oxidation potential was calibrated using ferrocene as the reference. The concentration of the iridium(III) complexes and supporting electrolyte were ~10^{-3} and ~10^{-1} M respectively. Thermal analyses were carried out on a meter Toledo TGA/SDTA 815 analyzer under a nitrogen atmosphere at a heating rate

of 10 °C/min.

Crystallography. The X-ray intensity data were collected on a Bruker SMART APEX-II CCD diffractometer using graphite monochromated Mo Kα radiation (λ = 0.71073 Å) at the temperature of 174 K. The structures were solved using a SHELXS-97 and refined by a full-matrix least-squares calculation on F^2 using SHELXL-97.[6] All non-hydrogen atoms were refined anisotropically except O atoms of the disordered water molecules. The water H atoms were not found out because of the disordering in the lattice. The other hydrogen atoms were placed in ideal positions and were riding on their respective carbon atoms (B_{iso} = 1.2 B_{eq} and 1.5 B_{eq}).

Results and Discussion

Synthesis and Characterization. The reaction of pqx and $IrCl_3 \cdot nH_2O$ in 2-ethoxyethanol afforded the μ-chloro-bridged dimer complex $[(pqx)_2Ir(\mu\text{-}Cl)]_2$. The treatment of $[(pqx)_2Ir(\mu\text{-}Cl)]_2$ dimer with a mprz ligand in the presence of Na_2CO_3 yielded the monomeric complex $[(pqx)_2Ir(mprz)]$ (**1**). Similarly, complex $[(pqx)_2Ir(prz)]$ (**4**) was obtained using prz chelate ligand instead of the mprz ligand. The monomeric iridium(III) complexes, $[(dmpqx)_2Ir(mprz)]$ (**2**), $[(dfpqx)_2Ir(mprz)]$(**3**), $[(dmpqx)_2Ir(prz)]$ (**5**) and $[(dfpqx)_2$-Ir(prz)] (**6**), were also synthesized for subtle tuning of the emission wavelength. Scheme 1 outlines the synthetic protocol for the ligands and phosphorescent iridium(III) complexes. All iridium(III) complexes were highly soluble in chlorinated solvents. ^{1}H NMR spectral analyses were consistent with the proposed structures. Complex **2** was examined further using single-crystal X-ray analysis to establish its three dimensional structure.

A single crystal of complex **2** was grown by the diffusion of hexane into a concentrated dichloromethane solution and

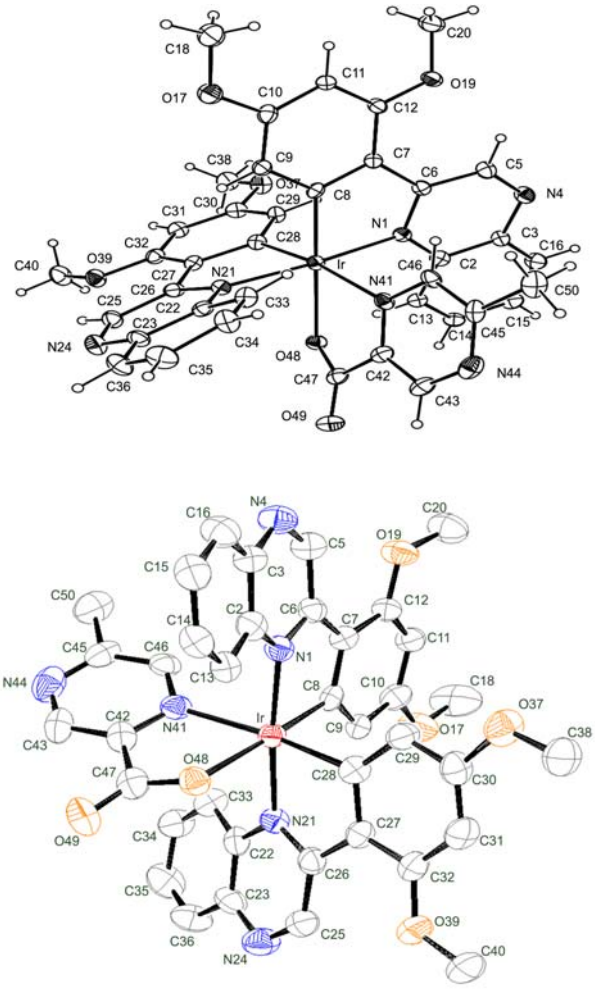

Figure 1. Molecular structure of $(dmpqx)_2Ir(mprz)$ (**2**), showing the atom-numbering scheme. The thermal ellipsoids represent the 30% probability limit. The hydrogen atoms were omitted for clarity.

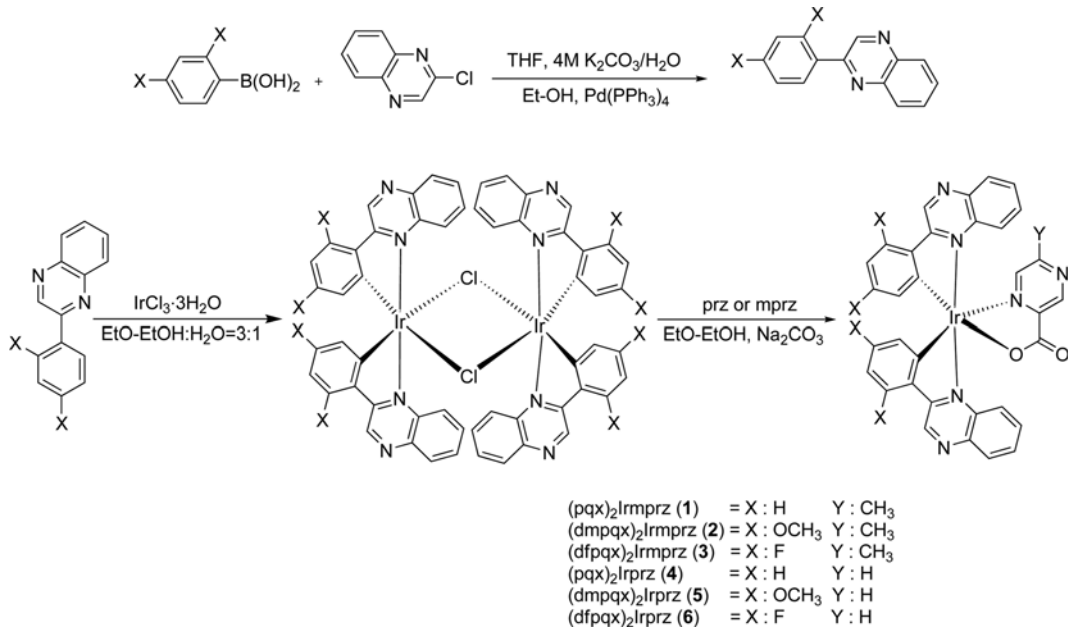

Scheme 1. Synthetic route for ligand and iridium(III) complexes **1**-**6**.

Table 1. Crystal data and structure refinement for complex **2**

Complex	(dmpqx)$_2$Ir(mprz) (**2**)
Chemical formula	$C_{38}H_{31}N_6O_6Ir{\cdot}2CH_2Cl_2{\cdot}H_2O$
Formula weight	1047.76
Temperature	174(2) K
Crystal system, Space group	monoclinic, $P2_1/c$
a (Å), α (°)	10.690(2), 90
b (Å), β (°)	27.137(5), 94.06(3)
c (Å), γ (°)	15.071(3), 90
Volume	4360.8(15) Å^3
Z, Calculated density	4, 1.596 Mg/m^3
Absorption coefficient	3.361 mm^{-1}
F(000)	2080
Crystal size	0.15 × 0.15 × 0.14 mm
θ range for data collection	1.55 to 28.29
Reflections collected	43669
Independent reflections	10809 [R_{int} = 0.0811]
Final R indices [$I > 2\sigma(I)$]	R_1 = 0.0623, wR_2 = 0.1502
R indices (all data)	R_1 = 0.1300, wR_2 = 0.1817
Data/restraints/parameters	10809/0/524
Goodness-of-fit on F^2	1.033
Largest diff. peak and hole	2.343 and −1.905 e Å^{-3}

its structure was confirmed unambiguously by X-ray crystallography. Figure 1 shows the molecular structure of complex **2**. Table 1 presents the X-ray crystallographic data and Table 2 lists the selected bond lengths and bond angles. As shown in Figure 1, complex **2** showed distorted octahedral geometry around the iridium metal ion, consisting of two cyclometalated dmpqx ligands and one mprz ligand. The dmpqx ligands adopt a mutual eclipse configuration with their coordinated nitrogen atoms, N(1) and N(21), and carbon atoms, C(8) and C(28), being in the *trans* and *cis* orientation, respectively. The methylpyrazine carboxylate is located at a unique position opposite to the carbon atoms of the dmpqx ligands. This *trans* N-N and *cis* C-C ligand arrangement is the same as those of the parent phenylpyridine ligands in the μ-chloro-bridged dimer complex [(ppy)$_2$Ir(μ-Cl)]$_2$,[7] iridium diketonate complexes such as (ppy)$_2$Ir(acac)[8] and even the associated derivatives with the pyrazinecarboxylate ancillary ligand. This suggests that the pyrazinecarboxylate ligand in this case is attached to the metal *via* a simple replacement of both chloride ligands. The *cis* C-C arrangement is expected from the fact that the *trans* C-C is higher in energy and more labile due to the electron-rich σ-phenyl ligand, which is referred to as "transphobia".[9] The bond angles in the iridium octahedron vary from 75.7(3) to 103.1(2)° and from 168.6(3) to 174.5(3)° as shown in Table 2. The bite angles at iridium are 79.6(3) and 80.0(3)° because the cyclometalated ligands are distinctly smaller than those of similar complexes.[8] The Ir-N1 (2.061(7) Å) and Ir-N21 (2.060(7) Å) bond lengths are shorter than 2.149(7) Å observed in Ir-N41, suggesting a stronger *trans* influence of the phenyl ring compared to the pyridyl groups, which have a trans N-N configuration. The strong *trans* influence of the phenyl group resulted in a longer Ir-O48 bond length (2.178(6) Å) than the mean Ir-O values of 2.088 Å reported in the Cambridge Crystallographic Database.[10]

Table 2. Selected bond lengths (Å) and angles (°) of (dmpqx)$_2$-Ir(mprz) (**2**)

Bond distances (Å)		Bond angles (°)	
Ir-C8	1.993(8)	C8-Ir-C28	92.1(3)
Ir-C28	2.012(9)	C8-Ir-N21	98.3(3)
Ir-N21	2.060(7)	C28-Ir-N21	79.6(3)
Ir-N1	2.061(7)	C8-Ir-N1	80.0(3)
Ir-N41	2.149(7)	C28-Ir-N1	95.1(3)
Ir-O48	2.178(6)	N21-Ir-N1	174.5(3)
		C8-Ir-N41	99.2(3)
		C28-Ir-N41	168.6(3)
		N21-Ir-N41	99.8(3)
		N1-Ir-N41	85.7(3)
		C8-Ir-O48	173.6(3)
		C28-Ir-O48	93.1(3)
		N21-Ir-O48	79.1(12)
		N1-Ir-O48	103.1(2)
		N41-Ir-O48	75.7(3)

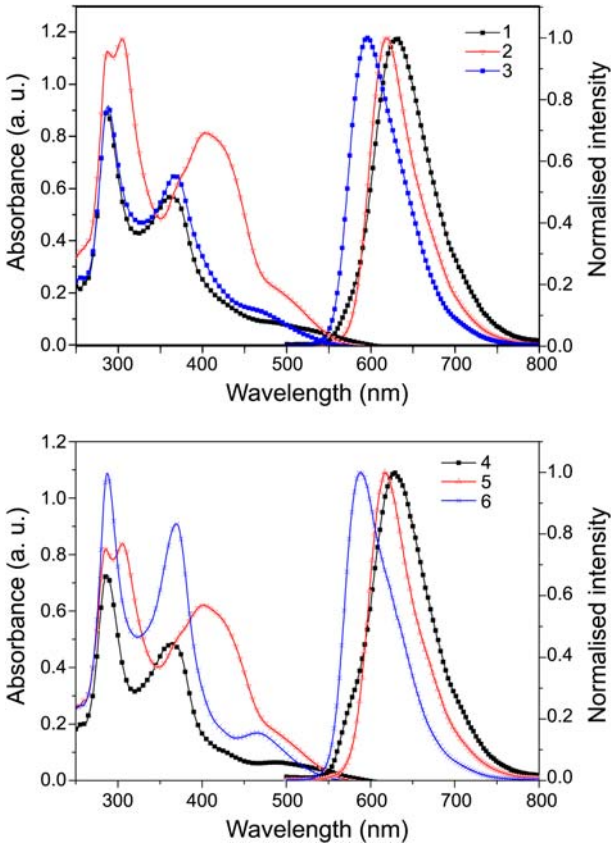

Figure 2. UV-vis. absorption and normalized emission spectra of complexes **1** to **6** in CH_2Cl_2 solution at room temperature

Photophysical Characterization. Figure 2 shows the UV-vis. absorption and photoluminescence (PL) spectra of the iridium(III) complexes **1-6**. Table 3 lists the resulting photophysical properties of the iridium complexes. All the complexes displayed strong absorption bands between 280 and 310 nm, which were assigned to π-π* ligand-centered transitions. In addition, spin-allowed metal-to-ligand charge

Table 3. Photophysical and electrochemical data of iridium complexes **1-6**

Complexes	Absorption[a] λ (nm) (ε, × 10^5 M^{-1} cm^{-1})	λ_{em} (nm)		Φ[c]	T_d[d] [°C]
		[a]RT/film[b]	77 K		
$(pqx)_2Ir(mprz)$ (**1**)	286 (3.58); 365 (2.22); 487 (0.34)	628/622	625	0.65	216
$(dmpqx)_2Ir(mprz)$ (**2**)	288 (4.49); 305 (4.68);373 (2.5); 406 (3.2); 492 (0.81)	620/617	612	0.72	262
$(dfpqx)_2Ir(mprz)$ (**3**)	288 (3.66); 368 (2.59); 472 (0.50)	596/607	592	0.82	262
$(pqx)_2Ir(prz)$ (**4**)	287 (2.91); 365 (1.92); 431 (0.38); 490 (025)	629/633	627	0.64	223
$(dmpqx)_2Ir(prz)$ (**5**)	286 (3.27); 305 (3.34); 372 (2.04); 401 (2.48); 490 (0.67)	616/615	614	0.76	240
$(dfpqx)_2Ir(prz)$ (**6**)	288 (4.32); 370 (3.62); 466 (0.67)	588/591	593	0.86	209

[a]All data was monitored in 1 × 10^{-5} M solution of iridium(III) complexes in CH_2Cl_2. [b]PMMA film doped with 5.0 wt % of Ir(III) complexes. [c]$Ir(ppy)_3$(0.40) was used as an external reference. [d]T_d indicates the decomposition temperature at a 5 wt% decrease.

transfer (^{1}MLCT) absorption, as evidenced from their molar extinction coefficients in the order 10^4~10^5 M^{-1} cm^{-1}, can be clearly distinguished in the region of 360-380 nm.[11] On the other hand, spin-forbidden triplet ^{3}LC and/or ^{3}MLCT transitions appear as lower energy absorption tails in the 460-500 region nm.[11]

Complexes **1-6** exhibited broad spectral emissions in the 588-630 region nm in a dichloromethane solution (~10^{-5} M) with high phosphorescence quantum efficiencies of 0.64-0.86. The PL spectra of these complexes in solid films were similar to those in solution. The significant overlap between the emission signal and the lowest energy absorption band in combination with broad and structureless spectral features was observed.

Complex **4**, $(pqx)_2Ir(prz)$ [λ_{max} = 628 nm], showed a 10-45 nm red-shift in emission compared to $(pqx)_2Ir(acac)$ [λ_{max} = 583 nm][5b], where acac is acetylacetonate and $(pqx)_2Ir(biimd)$ [λ_{max} = 618 nm][5a], where biimd is biimidazole. This shows that the ancillary ligand plays an important role in tuning the emission color from the $(pqx)_2Ir$ moiety and prz is an efficient ancillary ligand in red emission. Furthermore, highly quantum efficiencies of 0.64-0.86 were observed in complexes **1-6**. It was reported that a substituted nitrogen atom at the 4-position in 2-pyrazine carboxylic acid decreased the LUMO energy level in heteroleptic iridium complexes containing an ancillary pyrazinecarboxylate modulated ligand resulting in a red shift emission.[12] In addition, the reported iridium complexes showed highly efficient red emissions due to an inter-ligand energy transfer (ILET) process from ^{3}MLCT state to intra-ligand ^{3}LX energy state.[12,13a] On the basis of this reported study and the experimental observation of highly efficient red emissions in complexes (**1-6**), we suggest that a probable mechanism of phosphorescent emission is a highly efficient ILET process. An efficient intersystem crossing to ^{3}MLCT occurs after ^{1}MLCT excitation from the iridium moiety to the cyclometalating pqx ligand in the singlet manifold, followed by inter-ligand energy transfer to the ancillary ligand.

In addition, the emission bands of all complexes were blue shifted from room temperature to 77 K due to the rigidochromic effect.[14] The excited state at 77 K emits before solvent relaxation occurs, whereas room temperature emission occurs from the fully relaxed state within the lifetime of the excited state of the emitting molecule.

Table 4. Electrochemical properties of complexes **1-6**[a]

Complexes	E_{ox} (V)	E_{red} (V)	HOMO[b] (eV)	LUMO (eV)	E_{gap}[c] (eV)
$(pqx)_2Ir(mprz)$ (**1**)	1.52	-1.20; -1.47	-5.92	-3.47	2.45
$(dmpqx)_2Ir(mprz)$ (**2**)	1.16	-1.20; -1.44	-5.56	-3.06	2.50
$(dfpqx)_2Ir(mprz)$ (**3**)	1.83	-1.05; -1.30	-6.23	-3.71	2.52
$(pqx)_2Ir(prz)$ (**4**)	1.53	-1.05; -1.29	-5.93	-3.57	2.36
$(dmpqx)_2Ir(prz)$ (**5**)	1.19	-1.36; -1.54	-5.59	-3.19	2.40
$(dfpqx)_2Ir(prz)$ (**6**)	1.89	-0.94; -1.22	-6.29	-3.71	2.58

[a]All data was monitored in 1 × 10^{-3} M solution of iridium(III) complexes in CH_2Cl_2. [b]Potential values were reported *vs* Fc/Fc^+. [c]ΔE collected by UV-vis spectrophotometer.

Complex **3** bearing the 2,4-difluorophenyl group showed a ~32 nm hypsochromic shift in emission compared to complex **1**, which can be rationalized qualitatively by a decrease in the HOMO energy level due to the stronger electron-withdrawing character of the fluorine atom at the *ortho*- and *para*- positions.[13] Moreover, complex **2** resulted a 8 nm blue shift in emission peak maximum (λ_{max}) than complex **1**. In complexes **2** and **5**, the electron releasing substituent (-OCH_3) did not have a significant impact on emission comparing to complexes **3** and **6**. Similar phenomena were also observed in the iridium(III) complexes containing substituted quinoline, regardless of whether the substitutes in the 2-phenyl ring of the quinoline unit were electron- withdrawing -F or electron- releasing -OCH_3 groups.[15]

The thermal stability of complexes **1-6** were probed by thermogravimetric analysis (TGA), and exhibited 5% weight loss in the 209 to 262 °C range under a nitrogen atmosphere, as shown in Table 3, supporting its suitability for electronic device applications.

Electrochemical Properties. The electrochemical properties of the complexes were characterized by cyclic voltammetry (CV) in a methylene chloride solution to provide insight into the highest occupied molecular orbital (HOMO) energy levels of the complexes. All the iridium complexes showed irreversible oxidation potentials in the 1.16 to 1.89 V range and double quasi-reversible reduction waves with potentials ranges from −0.94 to −1.36 V and from −1.22 to −1.54 V. Oxidation occurred mainly at the iridium metal ion sites together with a contribution from the cyclometalated phenyl fragment, which led to a loss of electrochemical

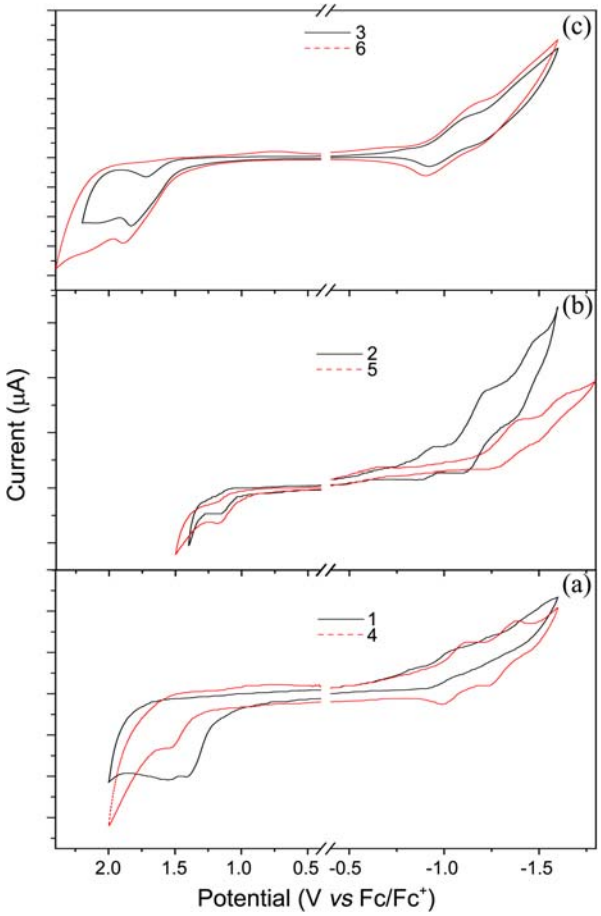

Figure 3. Cyclic voltammetry patterns of the six iridium(III) complexes (a) **1** and **4** (b) **2** and **5**, and (c) **3** and **6** in a 0.1 M $TBAPF_6$-CH_2Cl_2 solution at 298 K at a scan rate of 50 ms^{-1} using a glassy carbon electrode *versus* Ag/AgCl.

reversibility. On the other hand, double quasi-reversible reductions occurred primarily on the stronger electron-accepting heterocyclic portion of the cyclcometalated C^N ligands.[16]

The oxidation potential of the Ir(III) complexes was translated into the HOMO using the equation, $E_{HOMO} = -(E_{ox} + 4.4)$ eV, where E_{ox} is the onset oxidation potential and the energy band gap (ΔE_{gap}) of the iridium(III) complexes deduced from the absorption edge of the absorption spectra from $\Delta E_{gap} = 1240/\lambda_{edge}$, where λ_{edge} is the onset value of the absorption spectrum in the film.[17] The LUMO energy levels were estimated from the HOMO values and optical band gaps (ΔE_{gap}) by $E_{LUMO} = E_{HOMO} + \Delta E_{gap}$. Table 4 summarizes the electrochemical data relative to a ferrocenium/ferrocene redox couple and the energy levels of the Ir(III) complexes.

The oxidation potential of complex **3** containing electron withdrawing fluorine atoms on the 2,4-position of the phenyl ring was 1.83 V, which was shifted positively by 0.31 V compared to complex **1**, whereas complex **2** containing electron-donating -OCH_3 groups on 2,4-position of the phenyl ring showed an oxidation potential at 1.16 V. At the same time, the reduction potential of complex **3** was shifted from −1.20 V of complex **1** to −1.05 V. The CV data showed that an incorporation of electron withdrawing fluorine atoms on the phenyl ring led to a marked increase in the oxidation potential and a concomitant decrease in the reduction potential, whereas the electron releasing -OCH_3 group on the phenyl ring decreased the oxidation potential and increased the reduction potential.[18] This shows that the introduction of electron withdrawing groups on the phenyl ring reduces the HOMO energy level, resulting in a blue shift in an emission. The presence of electron donating -CH_3 group at the 5-position on the mprz ligand shifts the oxidation potentials to lower values than the prz ligand. Accordingly, the electron enrichment of the metal centered redox site destabilized the HOMO energy level, resulting in making the iridium(III) metal ion easier to oxidize.

Conclusions

A series of six heteroleptic cyclometalated iridium(III) complexes **1-6** bearing 2-(2,4-substituted phenyl)-quinoxaline and 2-pyrazinecarboxylate (prz) or 5-methyl-2-pyrazinecarboxylate (mprz) ligands as red triplet emitters were synthesized. The complexes incorporated two substituted cyclometalated ligands with an extended π system with fused heteroaromatic rings and one chromophoric ancillary ligand to counterbalance the energy gap suited for red emission. The optical and electrochemical properties were examined and compared with those reported for $(pqx)_2Ir(L^X)$, where L^X = acetylacetonate (acac) or biiidazole (biimd) complexes. The prz ancillary ligand plays an important role in the red-shifted emission in the heteroleptic cyclometallated iridium complexes due to the ILET process. X-ray diffraction of complex $(dmpqx)_2Ir(prz)$ (2) showed that the complex exists as a descriptive monomer showing a distorted octahedral symmetry around the iridium metal ion with no intermolecular interactions in the solid. These complexes exhibited high emission quantum yields (Φ = 0.64-0.86) suitable for red emitting phosphors for OLEDs applications. The color tuning of heteroleptic cyclometallated iridium(III) complexes was achieved by relative energy level control of the main and ancillary ligands.

Supplementary Material. Crystallographic data for the structure reported here have been deposited with the Cambridge Crystallographic Data Center (Deposition No. CCDC-671926 for [$(dmpqx)_2Ir(mprz)$] (**2**)). The data can be obtained free of charge *via* www.ccdc.cam.ac.uk/deposit (or from the CCDC, 12 Union Road, Cambridge CB2 1EZ, UK; Fax: +44-01223 336033; E-mail: deposit@ccdc.cam.ac.uk).

Acknowledgments. This work was supported by the research fund of Samsung Display, Korea.

References

1. (a) Chi, Y.; Chou, P.-T. *Chem. Soc. Rev.* **2010**, *39*, 638. (b) Xiao, L.; Chen, Z.; Qu, B.; Luo, J.; King, S.; Gong, Q.; Kido, J. *Adv. Mater.* **2011**, *23*, 926. (c) Ulbricht, C.; Beyer, B.; Friebe, C.; Winter, A.; Schubert, U. S. *Adv. Mater.* **2009**, *21*, 4418. (d) Wiegmann, B.; Jones, P. G.; Wagenblast, G.; Lennartz, C.; Munster,

I.; Metz, S.; Kowalsky, W.; Johannes, H.-H. *Organometallics*, **2012**, *31*, 5223. (e) Tavasli, M.; Moore, T. N.; Zheng, Y.; Bryce, M. R.; Fox, M. A.; Griffiths, G. C.; Jankus, V. I.; Al-Attar, H. A.; Monkman, A. P. *J. Mater. Chem.* **2012**, *22*, 6419.
2. Bera, N.; Cumpustey, N.; Burn, P. L.; Samuel, I. D. W. *Adv. Funct. Mater*. **2007**, *17*, 1149.
3. Grushin, V. V.; Herron, N.; LeCloux, D. D.; Marshall, W. J.; Petrov, V. A.; Wang, Y. *Chem. Commun.* **2001**, 1494.
4. Adachi, C.; Baldo, M. A.; Thompson, M. E.; Forrest, S. R. *J. Appl. Phys*. **2001**, *90*, 5048.
5. (a) Sengottuvelan, N.; Seo, H.-J.; Kang, S. K.; Kim, Y.-I. *Bull. Korean Chem. Soc*. **2010**, *31*, 2309. (b) Sengottuvelan, N.; Yun, S.-J.; Kang, S. K.; Kim, Y.-I. *Bull. Korean Chem. Soc*. **2011**, *32*, 4321.
6. Sheldrick, G. M. *Acta Cryst.* **2008**, *A64*, 112.
7. Graces, F. O.; King, K. A.; Watts, R. J. *Inorg. Chem.* **1988**, *27*, 3464.
8. Lamansky, S.; Djurovich, P.; Murphy, D.; Abdel-Razzaq, F.; Lee, H.; Adachi, C.; Burrows, P. E.; Forrest, S. R.; Thompson, M. E. *J. Am. Chem. Soc*. **2001**, *123*, 4304.
9. Vicente, J.; Arcas, A.; Bautista, D.; Arllano, M. C. R. *J. Organomet. Chem.* **2002**, *663*, 164.
10. Allen, F. H.; Davies, J. E.; Galloy, J. J.; Johnson, O.; Kennard, O.; Macrae, C. F.; Mitchell, E. M.; Mitchell, G. F.; Smith, J. M.; Watson, D. G. *J. Chem. Inf. Comput. Sci.* **1991**, *31*, 187.
11. Wilde, A. P.; King, K. A.; Watts, R. J. *J. Phys. Chem.* **1991**, *95*, 629.
12. You, Y.; Park, S. Y. *J. Am. Chem. Soc.* **2005**, *127*, 12438.
13. (a) You, Y.; Kim, K. S.; Ahn, T. K.; Kim, D.; Park, S. Y. *Phys. Chem. C* **2007**, *111*, 4052. (b) Hwang, F. M.; Chen, H.; Chen, P.; Liu, C.; Chi, Y.; Shu, C.; Wu, F.; Chou, P.; Peng, S.; Lee, G. *Inorg. Chem.* **2005**, *44*, 1344.
14. Tsuboyama, A.; Iwawaki, H.; Furugori, M.; Mukaide, T.; Kamatani, J.; Igawa, S.; Moriyama, T.; Miura, S.; Takiguchi, T.; Okada, S.; Hoshino, M.; Uenno, K. *J. Am. Chem. Soc.* **2003**, *125*, 12971.
15. Ding, J.; Gao, J.; Fu, Q.; Cheng, Y.; Ma, D.; Wang, L. *Syn. Met.* **2005**, *155*, 539.
16. (a) Lowry, M. S.; Bernhard, S. *Chem. Eur. J.* **2006**, *12*, 7970. (b) Dragonetti, C.; Falciola, L.; Mussini, P.; Righetto, S.; Roberto, D.; Ugo, R.; Valore, A. *Inorg. Chem.* **2007**, *46*, 8533.
17. Pu, B.; Wang, L.; Wa, H. B.; Yang, W.; Zhang, Y.; Liu, R. S.; Sun, M. L.; Peng, J.; Cao, P. *Chem. Eur. J.* **2007**, *13*, 7432.
18. Ma, A.-F.; Seo, H.-J.; Jin, S.-H.; Yoon, U. C.; Hyun, M. H.; Kang, S. K.; Kim, Y.-I. *Bull. Korean Chem. Soc.* **2009**, *30*, 2754.